

# Forecasting critical transitions using data-driven nonstationary dynamical modeling

Frank Kwasniok\*

College of Engineering, Mathematics and Physical Sciences, University of Exeter, Exeter EX4 4QF, United Kingdom

(Received 28 July 2015; revised manuscript received 3 November 2015; published 30 December 2015)

An approach to predicting critical transitions from time series is introduced. A nonstationary low-order stochastic dynamical model of appropriate complexity to capture the transition mechanism under consideration is estimated from data. In the simplest case, the model is a one-dimensional effective Langevin equation, but also higher-dimensional dynamical reconstructions based on time-delay embedding and local modeling are considered. Integrations with the nonstationary models are performed beyond the learning data window to predict the nature and timing of critical transitions. The technique is generic, not requiring detailed *a priori* knowledge about the underlying dynamics of the system. The method is demonstrated to successfully predict a fold and a Hopf bifurcation well beyond the learning data window.

DOI: [10.1103/PhysRevE.92.062928](https://doi.org/10.1103/PhysRevE.92.062928)

PACS number(s): 05.45.Tp, 05.90.+m

## I. INTRODUCTION

Complex dynamical systems subject to slowly varying external conditions may exhibit critical transitions or tipping points, that is, a qualitative change in the observed macroscopic behavior. An attractor or dynamical regime of the system becomes unstable and an alternative one emerges. Real-world examples of possibly huge socioeconomic importance are the climate system [1], ecological systems [2], medical applications [3], and financial markets [4]. Critical transitions in stochastic dynamical systems may be classified as bifurcation induced, noise induced, or rate induced [5]. A combination of several of these mechanisms in a particular system is possible.

In recent years, there has been much research activity focused on identifying early-warning signals of critical transitions in time series in order to detect, anticipate, or predict impending tipping points [6]. Indicators proposed so far are based on increasing autocorrelation (critical slowing-down) [7–9], increasing variance [10,11], detrended fluctuation analysis [12], trends in skewness [13], quasistationary probability densities and their modality [14–17], and bifurcation theory [18–20]. The most widely used approaches are still increasing autocorrelation and increasing variance. However, the issue of robustness as well as the sensitivity versus the specificity of such early-warning indicators are still under debate [21–23].

The present paper discusses a model-based approach to the prediction of critical transitions. The transition mechanism is explicitly modeled by deriving a nonstationary stochastic dynamical model of appropriate complexity from data. Integrations with this model beyond the learning data set are then used to predict future critical transitions in simulations of simple dynamical systems.

First, the methodology of nonstationary potential analysis to study one-dimensional bifurcations is developed (Sec. II) and exemplified in a Langevin equation with time-dependent drift taking the system through a fold bifurcation (Sec. III). Second, an approach to higher-dimensional and nongradient, nonstationary dynamical modeling is proposed (Sec. IV) and demonstrated in a relaxation oscillator undergoing a Hopf

bifurcation (Sec. V). The paper concludes with some general discussion (Sec. VI).

## II. ONE-DIMENSIONAL NONSTATIONARY POTENTIAL ANALYSIS

We consider a potentially high-dimensional, complex system which is subject to slow variations in its parameters or external conditions. A scalar variable  $x$  of the system is observed. The simplest framework for studying critical transitions is a nonstationary one-dimensional effective Langevin equation describing noise-driven motion in a time-varying potential landscape:

$$\dot{x} = -V'(x; t) + \sigma \eta. \quad (1)$$

$\eta$  is white Gaussian noise with zero mean and unit variance;  $\sigma$  is the standard deviation of the driving noise. The potential function is modeled by a polynomial with nonstationary coefficients:

$$V(x; t) = \sum_{i=1}^M i^{-1} a_i(t) x^i. \quad (2)$$

For a globally stable dynamics the degree  $M$  of the polynomial needs to be even. The expansion coefficients are represented in terms of prescribed time-dependent basis functions:

$$a_i(t) = \sum_{j=0}^{J_i} \alpha_{i,j} f_{i,j}(t). \quad (3)$$

We always set  $f_{i,0}(t) = 1$  for the time-independent part of the potential. Natural choices for the time-dependent functions  $f_{i,j}(t)$  for  $j > 0$  are trends [polynomial, that is,  $a_i(t) = \sum_{j=0}^{J_i} \alpha_{i,j} t^j$ , or other], (quasi-)periodicities [24] [represented by a superposition of Fourier modes, that is,  $a_i(t) = \alpha_{i,0} + \sum_{k=1}^{K_i} \alpha_{i,2k-1} \cos \omega_{i,k} t + \alpha_{i,2k} \sin \omega_{i,k} t$ , with  $J_i = 2K_i$ ], or other external covariates, which are given either in functional form or as a time series. We have

$$V'(x; t) = \sum_{i=1}^M \sum_{j=0}^{J_i} \alpha_{i,j} f_{i,j}(t) x^{i-1}. \quad (4)$$

One-dimensional Langevin dynamics with multiplicative noise have been used to model noisy on-off intermittency [25]

\*f.kwasniok@exeter.ac.uk

and financial market fluctuations [26] but these approaches do not incorporate the deterministic temporal variation of the drift term which is introduced here.

Given an equally sampled learning data set,  $\{x_0, x_1, \dots, x_N\}$ , with  $x_n = x(t_n)$ , the model parameters  $\alpha_{i,j}$  and  $\sigma$  are estimated according to the maximum likelihood principle. The sampling interval is  $\delta t = t_{n+1} - t_n$ . The Langevin equation is discretized according to the Euler-Maruyama scheme:

$$x_{n+1} = x_n - \delta t V'(x_n; t_n) + \sqrt{\delta t} \sigma \eta_n. \quad (5)$$

The likelihood function of the data set is

$$L(x_1, \dots, x_N | x_0) = \prod_{n=0}^{N-1} \frac{1}{\sqrt{2\pi} \sqrt{\delta t} \sigma} \exp\left(-\frac{1}{2} \frac{[x_{n+1} - x_n + \delta t V'(x_n; t_n)]^2}{\delta t \sigma^2}\right). \quad (6)$$

Maximization of the likelihood function leads to a least-squares problem with a unique solution given by the linear system of equations

$$\sum_{k=1}^M \sum_{l=0}^{J_k} A_{i,j,k,l} \alpha_{k,l} = b_{i,j}, \quad (7)$$

with

$$A_{i,j,k,l} = \delta t \sum_{n=0}^{N-1} f_{i,j,n} f_{k,l,n} x_n^{i+k-2} \quad (8)$$

and

$$b_{i,j} = -\sum_{n=0}^{N-1} f_{i,j,n} x_n^{i-1} (x_{n+1} - x_n). \quad (9)$$

The notation  $f_{i,j,n} = f_{i,j}(t_n)$  is used. The noise level is estimated as

$$\sigma^2 = \frac{1}{N \delta t} \sum_{n=0}^{N-1} [x_{n+1} - x_n + \delta t V'(x_n; t_n)]^2. \quad (10)$$

We have  $\sigma^{-2} A_{i,j,k,l} = -\partial^2 \log L / \partial \alpha_{i,j} \partial \alpha_{k,l}$ ; hence the observed Fisher information matrix of the estimation problem with respect to the parameters  $\alpha_{i,j}$  is  $\mathbf{I} = \sigma^{-2} \mathbf{A}$  and the error covariance matrix of the parameter estimates is  $\sigma^2 \mathbf{A}^{-1}$ . Here,  $\mathbf{A}$  is the square matrix formed from the elements  $A_{i,j,k,l}$  with the two summative indices  $(i,j)$  and  $(k,l)$ . This allows us to monitor a possible ill conditioning of the estimation problem due to overparametrization or model misspecification.

The present method can immediately also be applied to an unevenly sampled data set with sampling intervals  $\delta t_n = t_{n+1} - t_n$  as it is, without any need for prior interpolation of the data. In Eqs. (5) and (6), the constant time step  $\delta t$  just needs to be replaced with the variable time step  $\delta t_n$ , Eqs. (7) and (9) remain unchanged, and Eqs. (8) and (10) need to be replaced with

$$A_{i,j,k,l} = \sum_{n=0}^{N-1} \delta t_n f_{i,j,n} f_{k,l,n} x_n^{i+k-2} \quad (11)$$

and

$$\sigma^2 = \frac{1}{N} \sum_{n=0}^{N-1} \frac{[x_{n+1} - x_n + \delta t_n V'(x_n; t_n)]^2}{\delta t_n}. \quad (12)$$

As a by-product, the methodology contains a simple procedure for estimating a stationary dynamical potential model in the special case  $J_i = 0$  for all  $i$ .

The described parameter estimation method is consistent for  $\delta t_n \rightarrow 0$ . For finite sampling intervals  $\delta t_n$  we expect some bias in the estimates for  $\alpha_{i,j}$  and  $\sigma$ . Nevertheless, we here prefer this method for its simplicity. Alternatively, a method could be used which more accurately approximates the continuous propagator of the Langevin equation, e.g., a continuous Kalman filter [27,28]. The inconsistency could also be removed by defining the dynamical model from the outset as a discrete nonstationary stochastic polynomial map [ $x_{n+1} = \sum_{i=0}^M \sum_{j=0}^{J_i} \alpha_{i,j} f_{i,j}(t_n) x_n^i + \sigma \eta_n$ , with  $M$  odd]. However, then the illustrative association with a potential landscape would be lost. Moreover, the discrete model is applicable only to evenly sampled data. The discrete formulation is an option if the sampling intervals are really too large for Eq. (5) to be any reasonable approximation to Eq. (1).

### III. EXAMPLE: FOLD BIFURCATION FROM BISTABILITY TO MONOSTABILITY

We consider noise-driven motion in a nonstationary potential landscape which exhibits a bifurcation. The governing equation is

$$\dot{x} = -V'(x; t) + \sigma \eta. \quad (13)$$

The potential is given by

$$V(x; t) = \frac{1}{4} x^4 - \frac{1}{2} x^2 - F(t)x, \quad (14)$$

with  $F(t) = \frac{t}{500} F_0$  and  $F_0 = 2\sqrt{3}/9$ . The noise level is  $\sigma = 0.9$ . The system is considered in the time interval  $[0, 800]$ . The Langevin equation is integrated in time using the Euler-Maruyama scheme with step size  $h = 10^{-4}$ . Figure 1(a) shows a sample trajectory of the system. At  $t = 0$ , there is a symmetric two-well potential with local minima at  $x = -1$  and  $x = 1$  separated by a potential barrier, and the trajectory flickers between the two metastable states. Then the ramped forcing  $F(t)$  is applied to the symmetric potential system; one well gradually shallows and the other deepens. The deeper well becomes more and more preferred. At  $t = 500$ , a transition from bistability to monostability occurs via a fold bifurcation.

The time interval  $[0, 300]$  is used as the learning data window. The sampling interval is  $\delta t = 0.025$ ; the length of the learning data set is  $N = 12000$ . The potential function for the analysis is chosen as

$$V(x; t) = (\alpha_{1,0} + \alpha_{1,1} t^*) x + \frac{1}{2} \alpha_{2,0} x^2 + \frac{1}{3} \alpha_{3,0} x^3 + \frac{1}{4} \alpha_{4,0} x^4, \quad (15)$$

with rescaled time  $t^* = \frac{t}{500}$ ; the initial symmetry of the potential is not prescribed. The true parameter values are  $\alpha_{1,0} = 0$ ,  $\alpha_{1,1} = -F_0 \approx -0.38$ ,  $\alpha_{2,0} = -1$ ,  $\alpha_{3,0} = 0$ , and  $\alpha_{4,0} = 1$ .

The estimated parameter values with standard errors are  $\alpha_{1,0} = 0.04 \pm 0.12$ ,  $\alpha_{1,1} = -0.41 \pm 0.30$ ,  $\alpha_{2,0} = -1.02 \pm 0.13$ ,  $\alpha_{3,0} = -0.02 \pm 0.07$ , and  $\alpha_{4,0} = 0.97 \pm 0.08$ . The noise

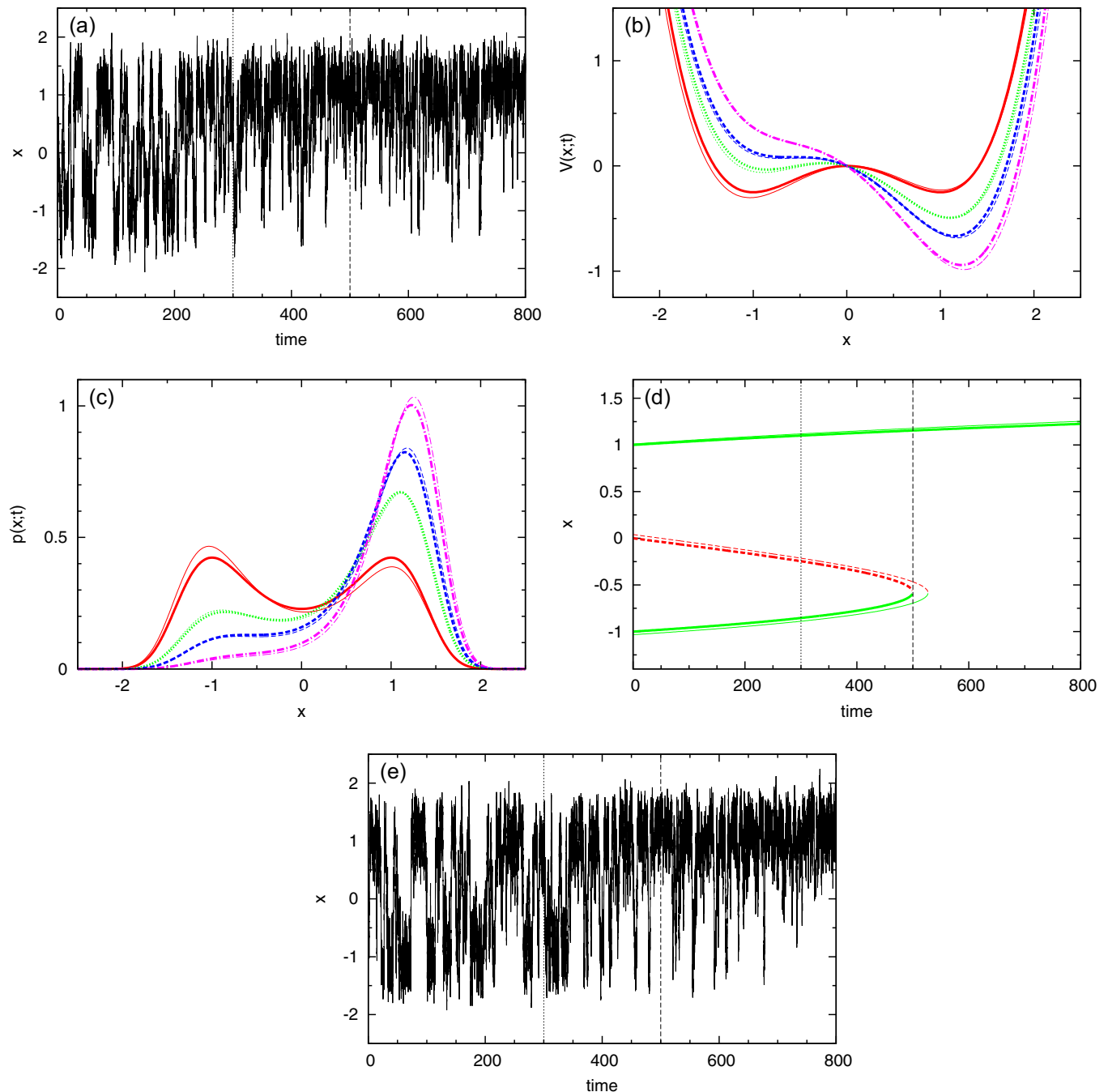


FIG. 1. (Color online) Noise-driven motion in a potential landscape with fold bifurcation from bistability to monostability. (a) Time series of the system. The short-dashed vertical line indicates the end of the learning data window, and the long-dashed vertical line shows the bifurcation point. (b) True (thick lines) and reconstructed/predicted (thin lines) potential at  $t = 0$  [solid (red) line],  $t = 300$  [dotted (green) line],  $t = 500$  [dashed (blue) line], and  $t = 800$  [dot-dashed (purple) line]. (c) True (thick lines) and reconstructed/predicted (thin lines) quasistationary probability density at  $t = 0$  [solid (red) line],  $t = 300$  [dotted (green) line],  $t = 500$  [dashed (blue) line], and  $t = 800$  [dot-dashed (purple) line]. (d) Bifurcation diagram as a function of time of the true (thick) and reconstructed/predicted (thin) systems. Solid (green) lines indicate stable states; dashed (red) lines, unstable states. The short-dashed vertical line indicates the end of the learning data window, and the long-dashed vertical line shows the bifurcation point. (e) Time series of the data-based model. The short-dashed vertical line indicates the end of the learning data window, and the long-dashed vertical line shows the bifurcation point.

level is estimated as  $\sigma = 0.89$ . Biases in the parameters due to the finite sampling interval appear to be small, although the sampling interval is not infinitesimal ( $\delta t = 0.025 \gg h = 0.0001$ ). Figures 1(b) and 1(c) display the potential and the quasistationary probability density {given

as  $p(x;t) \sim \exp[-2V(x;t)/\sigma^2]$  of the true system and as reconstructed/predicted by the data-based model at the beginning and the end of the learning data window ( $t = 0$  and  $t = 300$ ), at the bifurcation point ( $t = 500$ ), and at some later point ( $t = 800$ ). The evolution of  $V(x;t)$  and  $p(x;t)$  over time

is very accurately captured by the model. Figure 1(d) shows the bifurcation diagram of the system as a function of time. It is well reconstructed and predicted. The data-driven model predicts the fold bifurcation for  $t = 527$ . Figure 1(e) displays a sample trajectory of the estimated model. It is statistically indistinguishable from the true system trajectory in Fig. 1(a).

The length of the learning data set is quite large here and there is still considerable variability in the parameter estimates between samples (not shown). The results presented correspond to a typical case, close to a mean over many samples. Although the system is only one-dimensional, it is actually challenging to estimate the shape of the potential and, even more so, trends in it due to the high noise level. This is also evidenced by the relatively large uncertainty in the trend parameter  $\alpha_{1,1}$ , despite its being the only parameter describing the nonstationarity of the potential. An additional problem is the metastability of the system, which, even for large  $N$ , creates a substantial probability of observing an untypical sample trajectory, spending a disproportionate amount of time (relative to the quasistationary probability density) in the vicinity of one of the stable states, thus causing biases in the parameter estimates. The exact predicted timing of the bifurcation depends sensitively on the detailed parameter estimates. However, the qualitative feature of a fold bifurcation from bistability to monostability beyond the learning data window somewhere around  $t = 500$  is very robustly predicted, also already with a shorter learning data set.

#### IV. HIGHER-DIMENSIONAL NONSTATIONARY MODELING

The framework of an effective one-dimensional Langevin equation is appealing for its simplicity and the immediate interpretability of the potential landscape. However, the dynamics in a complex system may be high-dimensional and nongradient. It is not at all clear if they can be reduced to one dimension and this certainly depends on the choice of the variable  $x$ . For example, an oscillatory system crucially involves circulatory probability currents and cannot be reduced to a one-dimensional Langevin equation. We therefore make an attempt at higher-dimensional modeling.

Given only a time series of a scalar observable  $x$  of a higher-dimensional system the dynamics can be reconstructed using the technique of time-delay embedding [29–31] based on Takens's theorem. The method is rigorous for deterministic systems given the embedding dimension is chosen large enough; it can be adopted and still expected to be beneficial for stochastic systems. Here, a discrete nonstationary stochastic dynamical system is derived based on time-delay embedding and local polynomial modeling with time-dependent coefficients. Given an evenly sampled scalar time series of the system,  $\{x_n\}$ , with sampling interval  $\delta t$ , we form  $m$ -dimensional embedding vectors  $\mathbf{y}_n = (x_{n-(m-1)K}, \dots, x_n)$ ; the time delay is  $\tau = K\delta t$ . The (local) model for predicting the next data point is given as

$$x_{n+1} = a(t_n) + \sum_{i=0}^{m-1} b_i(t_n)x_{n-iK} + \rho_n\eta_n. \quad (16)$$

As before, the state and time dependences are separated. We here restrict ourselves to constant and linear terms in the

state variable  $x$ ; an extension to higher-order polynomials is straightforward. The model coefficients are modulated in terms of time-dependent basis functions:

$$a(t) = \sum_{j=0}^J \alpha_j f_j(t), \quad (17)$$

$$b_i(t) = \sum_{j=0}^{J_i} \beta_{i,j} g_{i,j}(t). \quad (18)$$

We set  $f_0(t) = 1$  and  $g_{i,0}(t) = 1$  for the time-independent part of the model. Choices for the basis functions  $f_j(t)$  and  $g_{i,j}(t)$  for  $j > 0$  are again trends, cycles, or prescribed external covariates.  $\eta$  is a stochastic process with zero mean and unit variance; a canonical choice is Gaussian and white. The state-dependent noise amplitude is  $\rho_n$ . The model can also be used in a deterministic mode by dropping the stochastic term, that is, replacing it with its mean 0 rather than sampling from its distribution. This is appropriate if the underlying system under consideration is known to be deterministic.

The model is applied locally in embedding space. For an embedding vector  $\mathbf{y}_n$  a neighborhood  $\mathcal{U}_n = \{\mathbf{y}_v\}$  is formed as the set of the  $R$  nearest neighbors in some chosen norm from a given learning data set of size  $N$ . The index  $v$  denotes the time index of the  $R$  nearest neighbors. The parameters  $\alpha_j$  and  $\beta_{i,j}$  are determined by least-squares regression on the embedding vectors  $\mathbf{y}_v$  in the neighborhood with their next data points  $x_{v+1}$ . They are found from the linear system of equations

$$\sum_{k=0}^J A_{j,k} \alpha_k + \sum_{i=0}^{m-1} \sum_{k=0}^{J_i} B_{j,i,k} \beta_{i,k} = c_j, \quad (19)$$

$$\sum_{k=0}^J C_{i,j,k} \alpha_k + \sum_{k=0}^{m-1} \sum_{l=0}^{J_k} D_{i,j,k,l} \beta_{k,l} = d_{i,j}, \quad (20)$$

with

$$A_{j,k} = \sum_{\mathcal{U}_n} f_{j,v} f_{k,v}, \quad (21)$$

$$B_{j,i,k} = C_{i,k,j} = \sum_{\mathcal{U}_n} f_{j,v} g_{i,k,v} x_{v-iK}, \quad (22)$$

$$D_{i,j,k,l} = \sum_{\mathcal{U}_n} g_{i,j,v} g_{k,l,v} x_{v-iK} x_{v-kK}, \quad (23)$$

$$c_j = \sum_{\mathcal{U}_n} f_{j,v} x_{v+1}, \quad (24)$$

$$d_{i,j} = \sum_{\mathcal{U}_n} g_{i,j,v} x_{v-iK} x_{v+1}. \quad (25)$$

The notation  $f_{j,v} = f_j(t_v)$  and  $g_{i,j,v} = g_{i,j}(t_v)$  is used. The state-dependent noise level is estimated from the residuals as

$$\rho_n^2 = \frac{1}{R} \sum_{\mathcal{U}_n} \left( x_{v+1} - \sum_{j=0}^J \alpha_j f_{j,v} - \sum_{i=0}^{m-1} \sum_{j=0}^{J_i} \beta_{i,j} g_{i,j,v} x_{v-iK} \right)^2. \quad (26)$$

Nonstationary local constant (or analog) modeling is obtained as a special case of the method when dropping the linear terms ( $\beta_{i,j} = 0$ ). The parameters  $\alpha_j$  are then obtained

from the linear system of equations

$$\sum_{k=0}^J A_{j,k} \alpha_k = c_j, \quad (27)$$

with  $A_{j,k}$  and  $c_j$  given by Eqs. (21) and (24).

If  $\eta$  is assumed to be white and Gaussian, least-squares regression is equivalent to maximum likelihood estimation locally in the neighborhood. Otherwise, or if the model is applied in the deterministic mode, least-squares estimation is a canonical procedure as a generic optimization principle.

The present approach is a natural extension of standard, that is, stationary, local polynomial modeling [32–34]. In the time-independent case ( $J = 0$  and  $J_i = 0$  for all  $i$ ) standard local linear modeling is recovered; when additionally dropping the linear terms ( $\beta_{i,0} = 0$ ) standard local constant (or analog) modeling [35] is recovered. Traditionally, these models are used only in the deterministic mode, in keeping with the assumption of a deterministic underlying dynamical system having generated the data.

### V. EXAMPLE: A RELAXATION OSCILLATOR UNDERGOING A HOPF BIFURCATION

The FitzHugh-Nagumo model augmented with stochastic noise is chosen as the test case. The equations of motion are

$$\varepsilon \dot{z} = z - \frac{z^3}{3} - w, \quad (28)$$

$$\dot{w} = z + c(t) + \sigma \eta. \quad (29)$$

$\eta$  is a white Gaussian noise with zero mean and unit variance;  $\sigma$  is the noise level. The time-scale separation parameter is fixed as  $\varepsilon = 0.05$ ; the parameter  $c$  is ramped according to  $c(t) = 0.9 + t/1500$ . For  $|c| < 1$  the deterministic system has a stable limit cycle; for  $|c| > 1$  there is a stable fixed point. At  $c = 1$  ( $t = 150$ ) the system undergoes a Hopf bifurcation. The model is integrated in time numerically using the Euler-Maruyama scheme with step size  $h = 10^{-4}$ .

The variable  $w$  is used as the scalar time series of the system, sampled at the time interval  $\delta t = 0.05$ . Embedding vectors of dimension  $m = 2$  are formed with time delay  $\tau = 0.5$ , corresponding to  $K = 10$ . We use a local linear model with a linear trend in time only in the constant term:

$$w_{n+1} = \alpha_0 + \alpha_1 t^* + \beta_{0,0} w_n + \beta_{1,0} w_{n-K} + \rho_n \eta_n. \quad (30)$$

The rescaled time is  $t^* = t/150$ . Neighborhoods consist of  $R = 50$  nearest neighbors in the Euclidian norm in embedding space. The results are fairly robust in the range from  $R = 30$  to  $R = 60$ . As a regularization of occasional ill-conditioned fits the regression equations are solved using the spectral decomposition of the system matrix and dropping eigenvalues and corresponding eigenvectors smaller than  $10^{-4}$  times the largest eigenvalue. The time interval  $[0, 100]$  is used as the learning data window. The learning data set has size  $N = 2000$ , covering the embedding vectors from  $\mathbf{y}_0 = (w_{-K}, w_0)$  to  $\mathbf{y}_{N-1} = (w_{N-1-K}, w_{N-1})$ , with corresponding next data points  $w_1$  to  $w_N$ .

We first consider the deterministic case ( $\sigma = 0$ ). Figures 2(a) and 2(b) show the learning data set and its

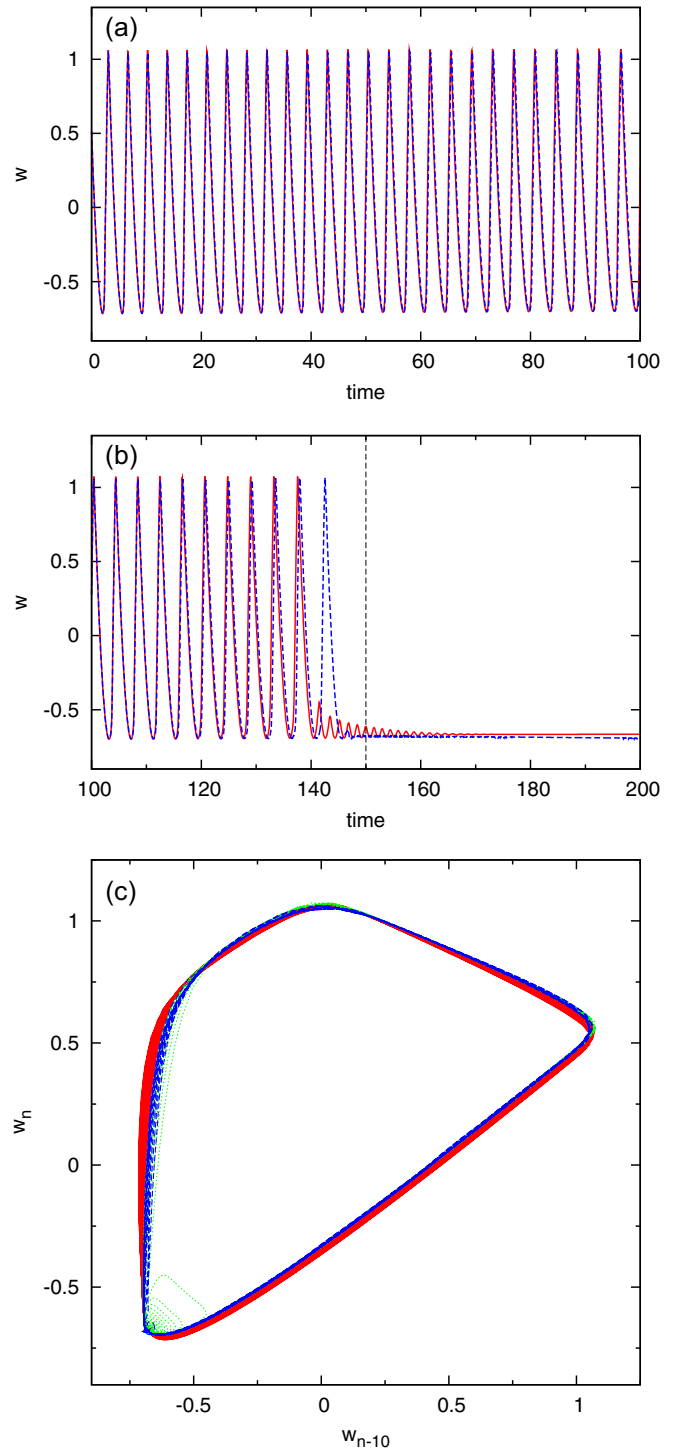


FIG. 2. (Color online) Relaxation oscillator without noise ( $\sigma = 0$ ) undergoing a Hopf bifurcation. (a) Learning data set of the true system [solid (red) line] and learning data set predicted by the data-based model [dashed (blue) line]. (b) Continuation of the learning data set from the true system [solid (red) line] and from the data-based model [dashed (blue) line]. (c) Nonstationary limit cycle in embedding space: trajectory of the learning data set from the true system [solid (red) line] and continuations from the true system [dotted (green) line] and the data-based model [dashed (blue) line].

continuation. The system performs self-sustained oscillations in a limit cycle. The amplitude of the limit cycle starts to

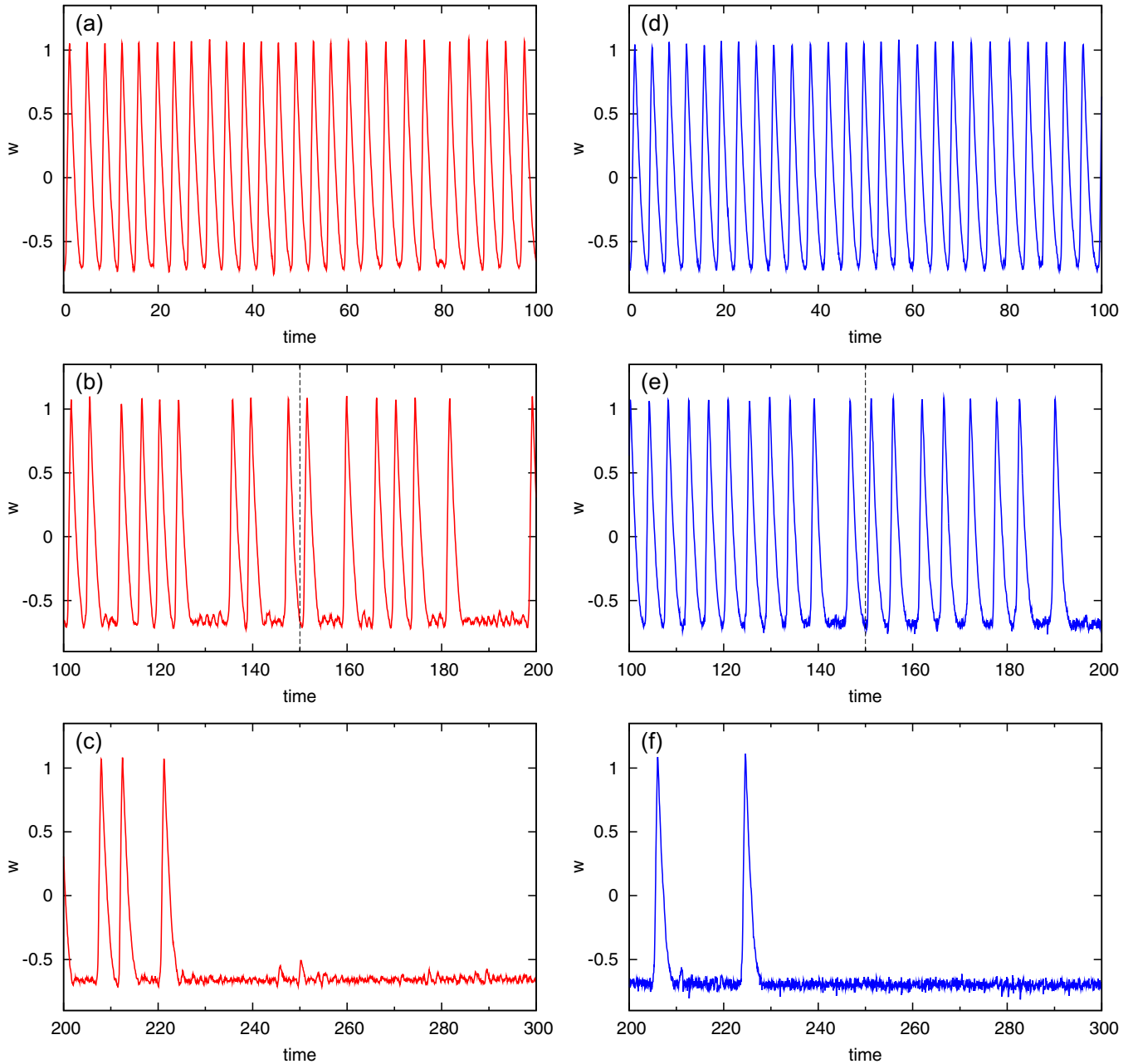


FIG. 3. (Color online) Relaxation oscillator with noise ( $\sigma = 0.035$ ) undergoing a Hopf bifurcation. (a) Learning data set from the true system. (b) Continuation of the learning data set. The dashed vertical line indicates the bifurcation point. (c) Further continuation of the time series from the true system. (d) Sample trajectory of the data-based model over the period of the learning data set. (e) Continuation of the sample trajectory. The dashed vertical line indicates the bifurcation point. (f) Further continuation of the sample trajectory.

shrink rapidly at about  $c = 0.994$ . Some transient behavior is visible shortly after the bifurcation point, as there the decay time scale of the fixed point is not small compared to the time scale of the ramping of the parameter  $c$ . The quality of the data-based model is assessed in-sample by predicting the learning data set. Here, the model is run in the deterministic mode, dropping the stochastic term. The one-step predictor is iterated starting with predicting  $w_1$  from the embedding vector  $\mathbf{y}_0 = (w_{-K}, w_0)$ . The current embedding vector to be predicted is excluded from forming the neighborhood. We are mainly interested in the overall statistical properties of the trajectory, but given the deterministic nature of the system

there is some interest in how well the trajectory of the true system can actually be predicted point by point. Therefore the trajectory of the data-based model is overlaid on the learning trajectory in Fig. 2(a). The reproduction is almost perfect; there is just a tiny phase shift at  $t = 100$ . Now the learning data set is continued into the future with the data-based model [Fig. 2(b)]. The trajectory is reinitialized at the end of the learning data window; that is, we start by predicting  $w_{N+1}$  from the embedding vector  $\mathbf{y}_N = (w_{N-K}, w_N)$  as given in the learning data set from the true system. The data-driven model accurately captures the timing of the transition well beyond the end of the learning data window and the subsequent quiescent phase of

the system. The model can also predict the system trajectory beyond the learning data window except for a small error in the period of the oscillations close to the bifurcation point. Figure 2(c) displays the time evolution of the limit cycle in embedding space. This sheds some light on how the method is working. The slight nonstationarity of the limit cycle, not visible by eye in the time series in Fig. 2(a), is picked up by the data-based model locally in embedding space and extrapolated into the future, eventually leading to the vanishing of the limit cycle. The difference between the true system and the data-based model is small, mainly visible in the last two spikes of the true system.

Now the system is studied at noise level  $\sigma = 0.035$ . Figures 3(a)–3(c) show a time series of the system. Under noise forcing the relaxation oscillator is still excitable for some time after the bifurcation point before entering the quiescent state. The data-based model is used in the stochastic mode, adding a random draw from a Gaussian with zero mean and variance  $\rho_n^2$  at each iteration step. A realization of the derived model starting at the beginning of the learning data window is displayed in Figs. 3(d)–3(f). The model correctly predicts the initial excitability of the system beyond the Hopf bifurcation point and the subsequent stabilization of the fixed point. Multiple realizations of the model (not shown) confirm this picture.

## VI. DISCUSSION

A method for predicting critical transitions from data based on nonstationary reconstruction of the underlying flow field

has been introduced and exemplified in simple systems. The technique is able to successfully predict a fold and a Hopf bifurcation well beyond the learning data window. Relaxation oscillators with time-varying stability and excitability properties appear to play a role in paleoclimatic transitions [36,37].

Unlike more traditional early-warning indicators such as increasing autocorrelation [8,9] and/or variance [10], the present method allows for genuine prediction, rather than just detection or anticipation, of the nature and the timing of an incipient transition. The present approach is more general and powerful than nonstationary probability density modeling [16,17]. It makes more efficient use of the data by exploiting information about the time evolution of system states rather than just the probability density. It is worth noting that the transition in the relaxation oscillator is not preceded by critical slowing-down or increasing variance, nor does it have a precursory signal in the probability density.

An interesting extension of the present work is critical transition modeling based on spatially extended data [38]. Some dimension reduction will then necessarily be involved in the analysis. A natural candidate for the essential modes of the system is principal components [39]. If the critical transition mechanism is rather low-dimensional, principal interaction patterns [40,41] may be an attractive choice, as they allow for simultaneous identification of the principal modes of the system and dynamical modeling of their time evolution.

- 
- [1] T. M. Lenton, H. Held, E. Kriegler, J. W. Hall, W. Lucht, S. Rahmstorf, and H. J. Schellnhuber, *Proc. Natl. Acad. Sci. USA* **105**, 1786 (2008).
  - [2] M. Scheffer, S. R. Carpenter, J. A. Foley, C. Folke, and B. Walker, *Nature* **413**, 591 (2001).
  - [3] P. E. McSharry, L. A. Smith, and L. Tarassenko, *Proc. Nature Med.* **9**, 241 (2003).
  - [4] D. Sornette and A. Johansen, *Physica A* **245**, 411 (1997).
  - [5] P. Ashwin, S. Wieczorek, R. Vitolo, and P. Cox, *Philos. Trans. R. Soc. London A* **370**, 1166 (2012).
  - [6] M. Scheffer, J. Bascompte, W. A. Brock, V. Brovkin, S. R. Carpenter, V. Dakos, H. Held, E. H. van Nes, M. Rietkerk, and G. Sugihara, *Nature* **461**, 53 (2009).
  - [7] C. Wissel, *Oecologica* **65**, 101 (1984).
  - [8] H. Held and T. Kleinen, *Geophys. Res. Lett.* **31**, L23207 (2004).
  - [9] V. Dakos, M. Scheffer, E. H. van Nes, V. Brovkin, V. Petoukhov, and H. Held, *Proc. Natl. Acad. Sci. USA* **105**, 14308 (2008).
  - [10] S. R. Carpenter and W. A. Brock, *Ecol. Lett.* **9**, 308 (2006).
  - [11] P. D. Ditlevsen and S. J. Johnsen, *Geophys. Res. Lett.* **37**, L19703 (2010).
  - [12] V. N. Livina and T. M. Lenton, *Geophys. Res. Lett.* **34**, L03712 (2007).
  - [13] V. Guttal and C. Jayaprakash, *Ecol. Lett.* **11**, 450 (2008).
  - [14] V. N. Livina, F. Kwasniok, and T. M. Lenton, *Climate Past* **6**, 77 (2010).
  - [15] V. N. Livina, F. Kwasniok, G. Lohmann, J. W. Kantelhardt, and T. M. Lenton, *Climate Dynam.* **37**, 2437 (2011).
  - [16] V. N. Livina, G. Lohmann, M. Mudelsee, and T. M. Lenton, *Physica A* **392**, 3891 (2013).
  - [17] F. Kwasniok, *Phys. Rev. E* **88**, 052917 (2013).
  - [18] C. Kuehn, *Physica D* **240**, 1020 (2011).
  - [19] J. M. T. Thompson and J. Sieber, *IMA J. Appl. Math.* **76**, 27 (2011).
  - [20] J. Sieber and J. M. T. Thompson, *Philos. Trans. R. Soc. London A* **370**, 1205 (2012).
  - [21] C. Boettiger and A. Hastings, *J. Roy. Soc. Interface* **9**, 2527 (2012).
  - [22] C. Boettiger and A. Hastings, *Proc. R. Soc. London B* **279**, 4734 (2012).
  - [23] T. M. Lenton, V. N. Livina, V. Dakos, E. H. van Nes, and M. Scheffer, *Philos. Trans. R. Soc. London A* **370**, 1185 (2012).
  - [24] Z. A. Thomas, F. Kwasniok, C. A. Boulton, P. M. Cox, R. T. Jones, T. M. Lenton, and C. S. M. Turney, *Climate Past* **11**, 1621 (2015).
  - [25] H. Nakao, *Phys. Rev. E* **58**, 1591 (1998).
  - [26] E. Canessa, *Eur. Phys. J. B* **22**, 123 (2001).
  - [27] F. Kwasniok and G. Lohmann, *Phys. Rev. E* **80**, 066104 (2009).
  - [28] F. Kwasniok, *Phys. Rev. E* **86**, 036214 (2012).
  - [29] N. H. Packard, J. P. Crutchfield, J. D. Farmer, and R. S. Shaw, *Phys. Rev. Lett.* **45**, 712 (1980).
  - [30] F. Takens, in *Dynamical Systems and Turbulence (Warwick 1980)*. Lecture Notes in Mathematics, Vol. 898, edited by D. A. Rand and L.-S. Young (Springer-Verlag, Berlin, 1981), pp. 366–381.

- [31] T. Sauer, J. Yorke, and M. Casdagli, *J. Stat. Phys.* **65**, 579 (1991).
- [32] J. D. Farmer and J. J. Sidorowich, *Phys. Rev. Lett.* **59**, 845 (1987).
- [33] G. Sugihara and R. M. May, *Nature* **344**, 734 (1990).
- [34] H. Kantz and T. Schreiber, *Nonlinear Time Series Analysis*, 2nd ed. (Cambridge University Press, Cambridge, UK, 2003).
- [35] E. N. Lorenz, *J. Atmos. Sci.* **26**, 636 (1969).
- [36] M. Crucifix, *Philos. Trans. R. Soc. London A* **370**, 1140 (2012).
- [37] F. Kwasniok, *Philos. Trans. R. Soc. London A* **371**, 20110472 (2013).
- [38] K. Gowda and C. Kuehn, *Commun. Nonlin. Sci. Numer. Simulat.* **22**, 55 (2015).
- [39] I. T. Jolliffe, *Principal Component Analysis* (Springer, Berlin, 2010).
- [40] K. Hasselmann, *J. Geophys. Res.* **93**, 11015 (1988).
- [41] F. Kwasniok, *Physica D* **92**, 28 (1996).